FEM Analysis of a New Electromechanical Converter with Rolling Rotor and Axial Air-Gap

Constantin UNGUREANU, Adrian GRAUR
Stefan cel Mare University of Suceava, 720229, Romania
costel@eed.usv.ro, adrian.graur@usv.ro

***Abstract*—The paper presents the modeling of a new type of electromechanical converter with rolling rotor (ECRR) in order to obtain an optimisation at functional level. The ECRR prototype comprises a stator composed of twelve magnetic poles and a disk-shaped rolling rotor made of ferromagnetic material, without windings. Each magnetic pole is made of an E-shaped magnetic system and a winding placed on its central column. The electromechanical converter with rolling rotor is analyzed through a magnetic field study with Flux2D® software in magnetostatic application. The field study examines the influence of the rotor thickness, axial air-gap size and current density on the magnetic attraction force that changes the position of the disk-shaped rolling rotor. Also, it is analyzed the variation of the magnetic attraction force for different inclination angles of the rolling rotor. The main advantage of the ECRR is represented by a low rotational speed without using mechanical gearboxes. The ECRR prototype can be used in photovoltaic panels tracking systems.**

***Index Terms*—angular velocity, air gap, finite element method, force measurement, friction.**

I. Introduction

Worldwide, there is a demand for electrical equipment to provide low rotational speed and high torque, characterized by constructive simplicity, low power consumption and high number of hours of operation without maintenance. The ECRR prototype analyzed in this paper was achieved by a patented solution [1]. The ECRR is characterized by originality and is on the border between electrical engineering and invention field. The originality is given by the constructive functional solution primarily related to low rotation speed obtained without using mechanical gearboxes. In literature, there are known some solutions characterized by low rotation speed and high torque. The best example relates to the interior rolling rotor motor analyzed in literature by finite element method [2-4]. Other equipment that provides low speed and high torque are using different types of RPM scalers which, in time, will eventually wear out.

The ECRR main advantages are: the disk-shape rotor is characterized by constructive simplicity and low cost of production due to lack of windings; no contact elements as in classic AC or DC electrical machines (rings, brushes etc.); operating noise is almost nonexistent.

The electromagnetic converter with rolling rotor is analyzed based on the finite element method (FEM) that provides high accuracy in calculation due to the large number of computational iterations. The used simulation program is Flux2D® and is a useful tool for analyzing and optimizing the proposed ECRR prototype. The paper aims at establishing the influence of variation of the main parameters (rotor thickness, axial air-gap, current density, inclination angle of the rolling rotor) on ECRR operation. The ECRR with axial air-gap analyzed in this paper represents a solution in photovoltaic panels tracking or in applications that require low rotation speed and high torque.

This paper has been financially supported within the project entitled „SOCERT. Knowledge society, dynamism through research", contract number POSDRU/159/1.5/S//132406. This project is co-financed by European Social Fund through Sectoral Operational Programme for Human Resources Development 2007-2013. Investing in people!".

II. ECRR General Theoretical Consideration

The ECRR investigations were based on the analogy with the electrostatic micromotor with rolling rotor and axial interstice [5]. An explanatory note to the operation principle of the ECRR, the electromagnetic version and the forces involved in operation are shown in Fig. 1.

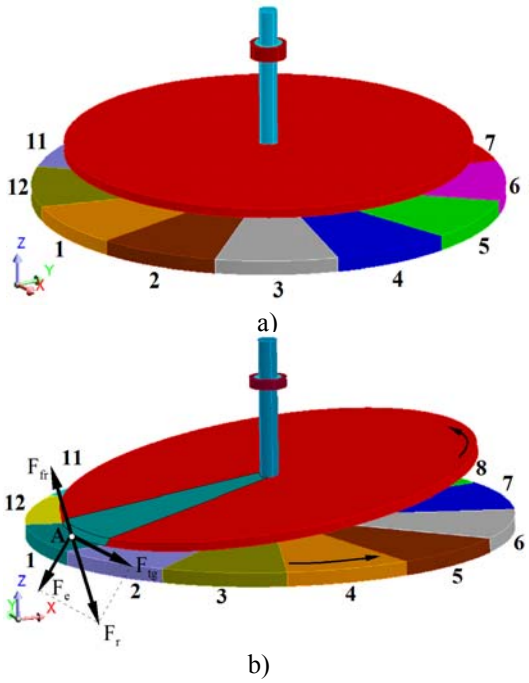

Figure 1. Overview of the ECRR principle of operation. The forces involved in operation: a) innactive disk-shaped rolling rotor; b) the rotor position when the magnetic pole ("1") is activated.

The ECRR operation is based on the difference between the rotor radius and the range of rolling over its route. During operation, the magnetic attraction force develops between the rolling rotor and each activated stator pole, which changes the direction of the rotor inclination in the direction of activated pole. The experimental model for which the 2D-FEM simulation was made is presented in various hypostases in Fig. 2. The stator consists of twelve windings. Each winding is placed on the center column of

Digital Object Identifier 10.4316/AECE.2015.04009

an E-shaped magnetic system. When all twelve stator windings are successively fed, a revolving magnetic field (Ω_T) appears and the rotor is rolling out under the influence of the magnetic attraction forces. If one single winding is activated, we have a rotor-stator contact point "A".

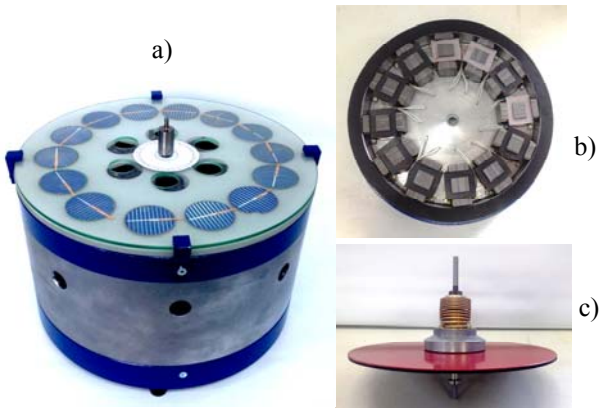

Figure 2. The ECRR prototype: a) general view; b) stator consisting of 12 magnetic poles; c) disk-shaped rotor made of ferromagnetic material.

In a complete cycle of the stator poles activation, with the angular velocity Ω_T, the mobile contact point rotates by an angle equal to 2π radians, in the same direction of the switching, in the stator poles plan. Thus, the rolling rotor assembly will perform a reduced angular displacement with the angular velocity, Ω_r.

The contact point moves around a circular path due to the tangential force F_{tg} that acts on the disk-shaped rotor. The rotation movement of the rotor is also possible due to the rolling friction force that occurs in the stator-rotor contact point. The maximum value of the tangential force depends on the stator-rotor contact conditions:

$$F_{tg\,max.} = \mu F_e \quad (1)$$

where μ is the coefficient of rolling friction.

The axial air-gap value (d) sets the time interval for which a complete rotation of the disk-shaped rotor is obtained, considering Ω_T with no variation. The force of magnetic attraction that changes the rotor inclination in the direction of activated winding, can be calculated using equation [6]:

$$F_e = (B^2 S_p)/2\mu_0 [N] \quad (2)$$

where: B is magnetic flux density at the magnetic pole surface; S_p is the surface of magnetic pole; μ_0 is the permeability of free space ($4\pi \cdot 10^{-7}$ H/m).

Changing the speed of rotation of the ECRR is based on the relationship [6]:

$$\Omega_r = \Omega_T / i \quad (3)$$

where, i represents the mechanical speed reduction ratio.

The gear ratio can be expressed by following equation if the slip between the rotor and the stator is neglected [5], [6]:

$$i = R_r / (R_r - R_s) \quad (4)$$

where, R_r and R_s represents the rotor radius and the rolling path radius respectively.

The radius of the circular route after which the contact point "A" of the rotor moves on the rolling path (see Fig. 1b) can be expressed depending on the α angle, through the relationship [4]:

$$R_s = \sqrt{R_r^2 + d^2} + (h_b - d)\sin\alpha \quad (5)$$

where, d represents the axial air-gap dimension, h_b represents the high of the spindle support of the rotor and α represent the inclination angle of the rotor in the direction of the rolling path.

For $\alpha = 0^0$, the disk-shaped rolling rotor has the position shown in Fig. 1a.

III. FEM Analysis

Out of the need to carry out more efficient electric equipments, it occurs the necessity to use the FEM modeling programs. FEM analysis is used in most applications that treat field problems and ensure high precision in this respect. If modeling is done effectively, the simulation results are close to the experimental ones. There are various studies that use the finite element method and were performed on various types of electrical equipment such as AC and DC electric machines [7-15] or electromagnetic actuators [16-18].

The FEM analysis of the ECRR prototype was carried out in a magnetostatic application of the Flux2D® software which represents a study of magnetic fields in systems where the currents are with not variation in time. Thus, for the knowledge of ECRR operation, a finite-element analysis is required.

It has been shown that the ECRR drive torque is influenced by the magnetic attraction force between the stator and the disk-shaped rotor, the rotor thickness and the current density value [6]. Also, the starting torque of the ECRR decreases as the angular velocity Ω_T increases [19]. In the same time, the starting torque can be increased by raising the current through stator windings or by reducing slipping phenomenon between stator and rotor [6]. The mechanical speed reduction ratio decreases simultaneously with the increase of axial air-gap and is dependent on the structural dimensions of the ECRR prototype (R, R_s, d, h_b and g_R), as stated in [6].

Using FEM-based simulation with Flux®2D software, it is possible to find out the influence of the geometrical and electrical parameters on the ECRR performance. Fig. 3 presents a 3D representation of the ECRR prototype that highlights the arrangement of the twelve electromagnetic actuators (EA) placed on an insulating support in regard to the disk-shaped rotor.

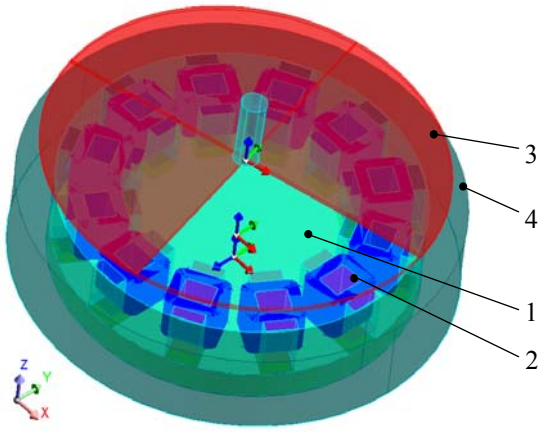

Figure 3. General view of the ECRR prototype – 3D representation: 1- insulating support; 2- electromagnetic actuator (EA); 3- disk-shaped rolling rotor; 4- rolling path.

In this paper, it will be analyzed through the finite element method only a part of the magnetic system of the

stator due to its symmetry that leads to the simplification of FEM analysis. Thus, the ECRR geometry has been divided into twelve slices, each of them being represented by one electromagnetic actuator. The computing model used in FEM analysis with highlighting of variable parameters g_R and d is presented in Fig. 4.

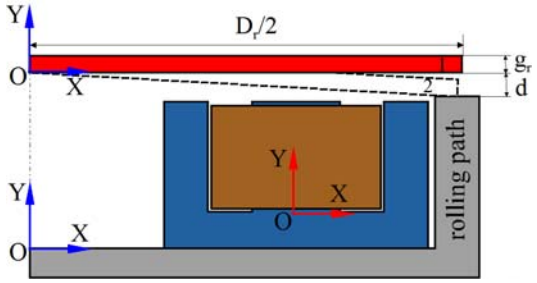

Figure 4. The geometry of the computing model: D_r- rotor diameter; g_r- rotor thickness; d- axial air-gap; 1- rotor position for $\alpha=0^0$; 2- rotor position for the possible maximum value of the α angle.

After creating the EA model to the real dimensions, it was made the mesh network and then where prescribed the properties of the materials. Later it was introduced the current density value obtained from calculations in order to achieve simulation. The FEM analysis was conducted with the rated parameters presented in Table I.

TABLE I. ECRR ELECTRICAL AND GEOMETRICAL PROPERTIES

	Description	Value	Symbol
Electrical	EA supply voltage [V]	12	U_n
	Consumption power [W]	12	P_n
	Winding inductance [H]	$64x10^{-3}$	L
	Number of turns on each pole	1090	N
	Ampere turns [At]	817,5	NI
	Number of stator poles	12	2p
	Wire diameter [m]	$0,45x10^{-3}$	d_i
	Maximum starting torque [Nm]	0,85	M_{max}
Geometrical	Rotor diameter [m]	0,310	D_r
	Rotor thicknees [m]	0,003	g_R
	Stator diameter [m]	0,340	D_s
	The height of ECRR [m]	0,200	H_{ec}
	The main dimensions of the EA [mm]	60x25x40	Lxlxh

The geometry was build to represent a single electromagnetic actuator and the corresponding rotor area. For the E-shaped magnetic system and the disk-shaped rotor has been used a nonlinear isotropic material with the flux density saturation J_s=1,5T and initial relative permeability μ_r=1500. The material is defined by an analytic magnetization curve B=f(H), shown in Fig. 5.

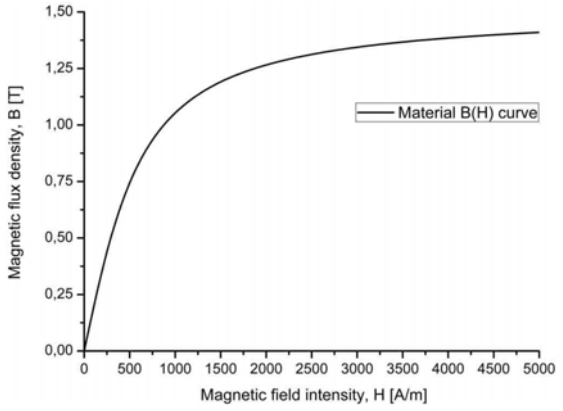

Figure 5. The magnetization curve of the material.

The geometry and the mesh adapted to the physics of the EA model are shown in Fig. 6. Details of the mesh in axial air-gap region are presented in Fig. 7.

To compute the attractive force on the air-gap, the Flux®2D software uses the following equation [20]:

$$F_S = \frac{1}{2\mu_0} \iint_S B^2 dS \quad (6)$$

The force exerted in axial plane is obtained, according to [20], by differentiating the magnetic energy of the electromagnetic actuator in relation to the rotor displacement:

$$F_S = -(\partial W / \partial \delta) \quad (7)$$

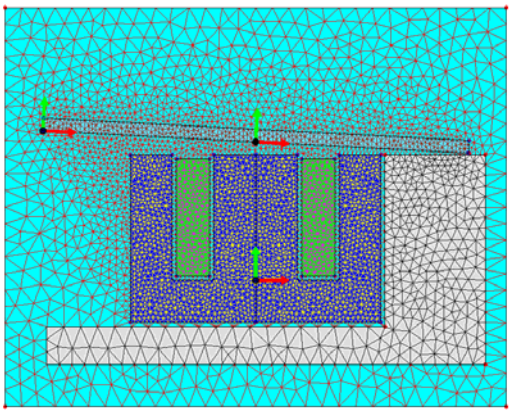

Figure 6. The geometry and the mesh of the computation domain of a single 2D FEM electromagnetic actuator.

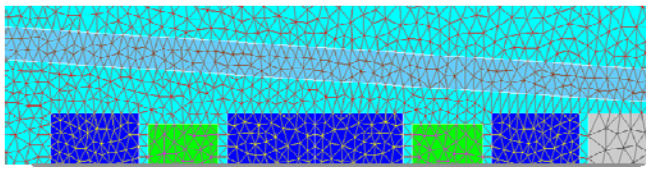

Figure 7. Detail of the mesh in the axial air-gap region.

By modeling the electromagnetic actuator, were analyzed a number of issues relating to:
- the magnetic flux density distribution in the two regions (E-shaped magnetic system and rotor);
- the magnetic attraction force that acts on the rotor for different values of g_R parameter and for different angles (α) of the rotor in regard to the rolling path;
- the current density variation through the winding.

IV. Analysis of the Post-Processing Results

After the solving of the computational model in magnetostatic application of Flux®2D software, the first results were obtained. The electromagnetic actuator (EA) was analyzed in two different situations. The first case analyzes the behavior of the EA considering the current density increase up to a maximum of 20 A/mm^2. The inclination angle of the rotor, relative to the rooling path, was considered with no variation ($\alpha=0^0$). The second case examines the real operation of ECRR, considering the current density with no variation (j=6,25 A/mm^2) and the inclination angle of the rotor between 0^0 to 7^0.

Before the post-processing results presentation of the two cases, in Fig. 8 and Fig. 9 are presented the computed vector quantities of the magnetic flux density on the rotor and magnetic system regions, for axial air-gap value of 10 mm. The value of the flux density does not exceed 0.81T for $\alpha=0^0$

and 1,61T for α=70. The arrows show the direction and magnitude of the magnetic flux density.

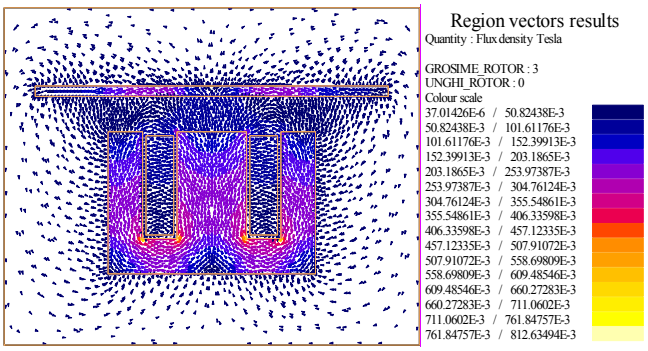

Figure 8. Flux density vectors distribution on the rotor and magnetic system regions for d=10mm, j=6,25A/mm^2, α=0^0.

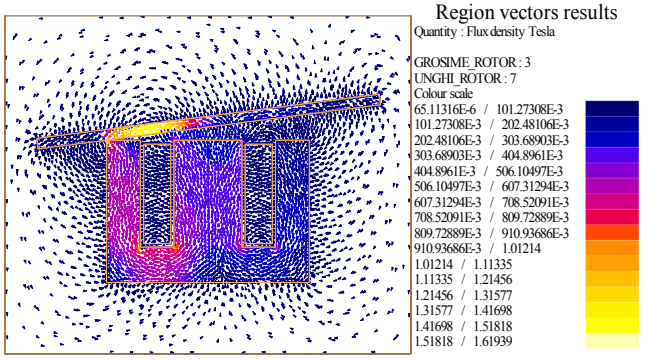

Figure 9. Flux density vectors distribution on the rotor and magnetic system regions for d=10mm, j=6,25A/mm^2, α=7^0.

Case 1

In the first case, the axial air-gap and the current density through the coil are parameterized. The rotor thickness remain constant at the 3mm value. The parameters used in FEM analysis, the interval of variation and the step values are shown in Table II.

TABLE II. THE VALUES OF THE PARAMETERS USED IN FEM ANALYSIS – CASE 1

Description	The interval of variation	The value of step
Rotor thickness, g_R [mm]	3	-
Axial air-gap, d [mm]	1 ÷ 10	1
Current density, j [A/mm^2]	4 ÷ 20	4
Inclination angle of the rotor, α [°]	0	-

The force acting on the rotor as function of the axial air-gap thickness and current density is presented in Fig. 10. As expected, the force increases with the increasing of *d* and *j* parameters, when the current density is with no variation. Using multiparametric analysis it is possible to reprezent a 3D dependence of mentioned parameters (Fig. 11).

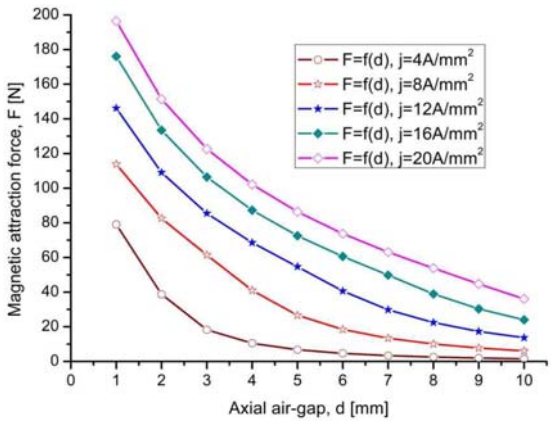

Figure 10. The variation of the magnetic attraction force as function of the *d* and *j* parameters. g_R = 3 mm, α=0^0.

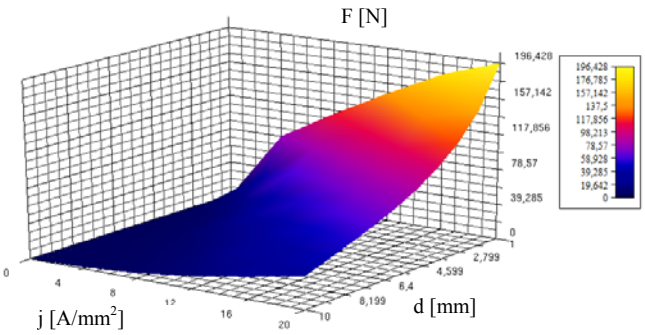

Figure 11. 3D dependence of the variation of the magnetic attraction force acting on the rotor as function of the *d* and *j* parameters. g_R = 3 mm, α=0^0.

Case 2

The second case analyzes the parameters variation obtained from the design calculations. Table III shows the assumptions considered for modeling.

TABLE III. THE VALUES OF THE PARAMETERS USED IN FEM ANALYSIS – CASE 2

Description	The interval of variation	The value of step
Rotor thickness [mm]	3 and 2÷6	1
Axial air-gap [mm]	1 ÷ 10	1
Current density [A/mm^2]	6,25	-
Inclination angle of the rotor $\alpha_{min} \div \alpha_{max}$ [^{0}]	0 ÷ 7	1

To determine the influence of the magnetic attraction force depending on thickness of the disk-shaped rotor, there were represented the F=f(g_r) characteristics for different possible inclination angles α and two distinct values of axial air-gap (10 mm and 6 mm). It is noted that, the magnetic attraction force value increases with the increasing of the inclination angle and not so significant with the increasing of the rotor thickness (Fig. 12).

For a value of 10 mm axial air-gap, it can be observed an insignificant increase of the magnetic attraction force for an angle of inclination between 0^0 and 4^0. An important increase of the attraction force can be seen for α=6^0 and α=7^0. A three-dimensional representation is shown in Fig. 13. The influence of the rotor thickness for d=6mm was also analyzed.

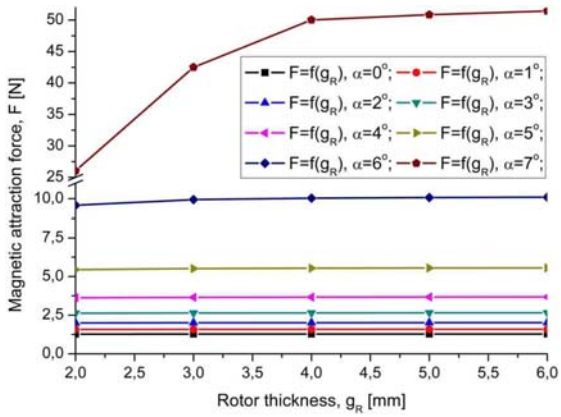

Figure 12. The variation of the magnetic attraction force as function of the g_R and α parameters. Axial air-gap value, d = 10 mm.

The F=f(g_r) characteristics are presented in Fig. 14, where it can be observed a significant increase of the magnetic attraction force for $\alpha = 3^0$ and $\alpha = 4^0$. A three-dimensional representation is shown in Fig. 15.

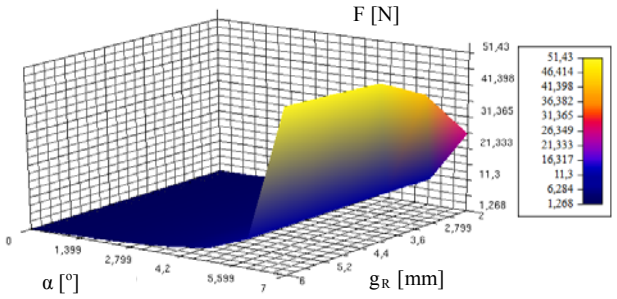

Figure 13. 3D dependence of the variation of the attraction force acting on the rotor as function of g_R and α parameters: j=6,25 A/mm^2, d=10mm.

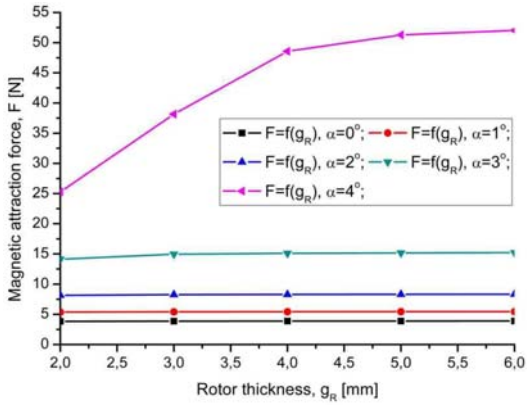

Figure 14. The variation of the magnetic attraction force as function of the g_R and α parameters. Axial air-gap value, d = 6 mm.

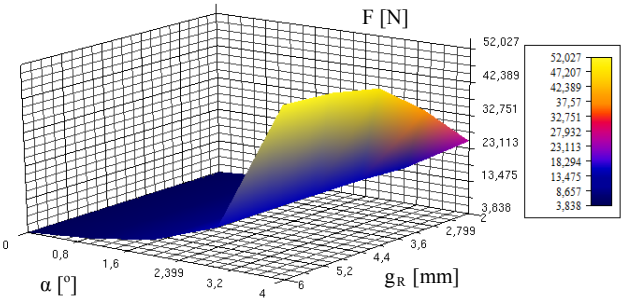

Figure 15. 3D dependence of the variation of the attraction force acting on the rotor as function of g_R and α parameters: j=6,25 A/mm^2, d=6mm.

The minimum and maximum values of the magnetic attraction force obtained for two different values of the axial air-gap are presented in Table IV.

If the rotor thickness (g_R) and current density (j) are both kept constant, the evolution of the magnetic attraction force that acts on the rotor can be found out. The simulation results confirm a growing attraction magnetic force as changing parameters α and d (Fig. 16).

TABLE IV. MAGNETIC ATTRACTION FORCE. MINIMUM AND MAXIMUM VALUES

Axial air-gap value d [mm]	Rotor thickness [mm]		Inclination angle of the rotor [°]		Magnetic attraction force [N]	
	$g_{R\ min}$	$g_{R\ max}$	α_{min}	α_{max}	F_{min}	F_{max}
10	2	6	0	7	1,26	51,43
6				4	3,83	52,02

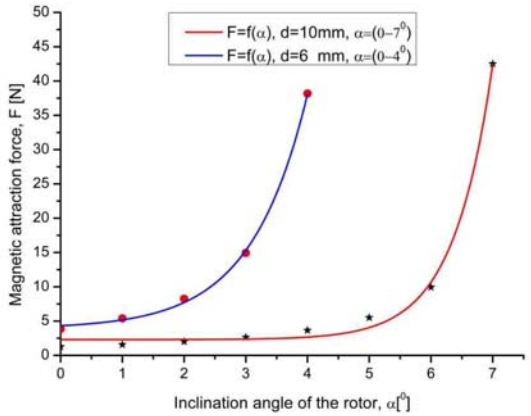

Figure 16. The variation of the magnetic attraction force as function of the α parameter. The g_R and d parameters is with no variation.

The variation of the flux density along the axial air-gap for the parameterized values of the inclination angle, for d=10mm and d=6mm, is presented in Fig. 17 and Fig. 18 respectively.

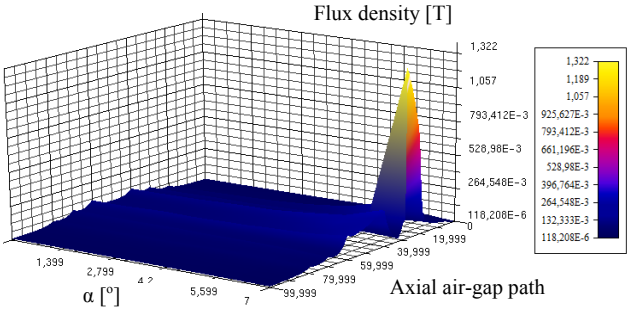

Figure 17. The variation of the flux density along the axial air-gap for the parameterized values of the inclination angle, α. Axial air-gap value, d=10 mm.

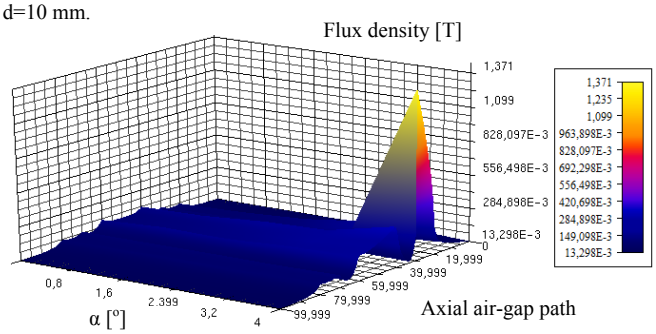

Figure 18. The variation of the flux density along the axial air-gap for the parameterized values of the inclination angle, α. Axial air-gap value, d=6 mm.

Of particular importance in this study is the flux density distribution in the axial air-gap area. First of all, it was defined the path in the axial axir-gap by numerical coordonates. After the path creation, we can plot the flux density along the air-gap for the parameterized values of the axial air-gap. The current density and the rotor thickness are considered with no variation. The flux density curve for an inclination angle of 0^0 and for two axial air-gap values are presented in Fig. 19. It can be observed the influence of the air-gap value on the flux density distribution along the considered path. When the inclination angle of the rotor has the maximum value, the air-gap flux density curve shows a different variation. In Fig. 20 the air-gap flux density curves are presented for $\alpha=4^0$ and $\alpha=7^0$, considering d=6mm and d=10mm respectively.

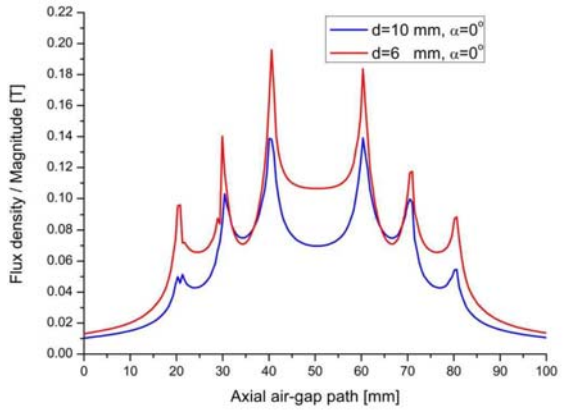

Figure 19. Flux density curve along the air-gap path, for the minimum value of the inclination angle. Current density j=6,25 A/mm^2. Rotor thickness g_R=3mm.

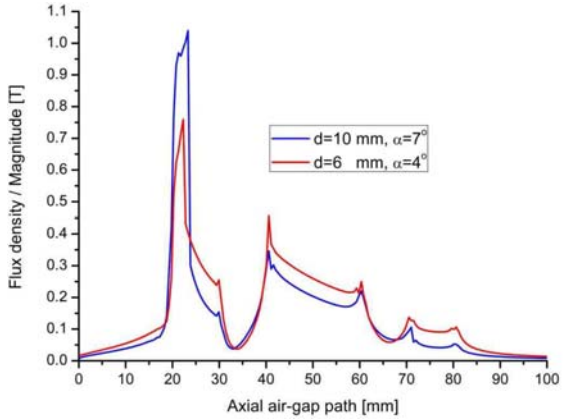

Figure 20. Flux density curve along the air-gap path, for the maximum possible value of the inclination angle. Current density j=6,25 A/mm^2. Rotor thickness g_R=3mm.

V. CONCLUSION

The 2D-FEM analysis was performed on a single electromagnetic actuator due to the constructive symmetry of the ECRR stator. The purpose scope of this paper is the study of the influence of the electrical and geometrical parameters on the magnetic attraction force. Four parameters have been modified: the current density, the axial air-gap, the rotor thickness and the inclination angle of the disk-shaped rotor.

Starting with the design data, the simulation was performed with Flux®2D software by which it has been verified the rotor thickness influence on the magnetic attraction force and its values were determined by the rotor possible position in respect with the rolling path.

The results of the modeling, for two distinct values of axial air-gap, have highlighted the magnetic attractive force variation with respect to the axial movement of the rotor. In both cases, it was observed a significant increase of the magnetic attraction force for that last two inclination angle values from the variation domain. If there is no variation for the rotor thickness and the axial air-gap, the magnetic attraction force increases with the increase of the inclination angle of the rolling disk-shaped rotor. This statement is valid for both axial air-gap values, of 10 mm and 6 mm respectively.

In conclusion, a 2D-FEM analysis is a useful and a nondistructive method to find out the influence of different parameters on the magnetic attraction force that acts on the disk-shaped rolling rotor.

REFERENCES

[1] D. Cernomazu, L. Mandici, C. Ungureanu, E.-D. Olariu, N. Sorea, et.al., "Solar motor," Patent no. 125573B1, 2011

[2] A. Arkkio, A. Biernat, B. Bucki, G. Kaminski, A. Niemenmaa, A. Smak, and P. Staszewski, "Finite Element Analysis for a Rolling-Rotor Electrical Machine," IEEE Transactions on Magnetics, Vol. 46, No. 8, August 2010, pp. 2727-2730

[3] R. Jürgen, H. R. Enslin Johan, D. Edwin Smith, "Digital Control and Optimization of a Rolling Rotor Switched Reluctance Machine," IEEE Transactions on Industry Applications, vol. 31, no. 2, march-april, 1995, pp. 338-344

[4] Z.P. Xia, Z.Q. Zhu, P.J. Monkhouse, D. Howe, "Electromagnetic Modeling of a Rolling Rotor Actuator," IEEE Transactions on Magnetics, vol. 29, no.6, pp. 3153–3155, November, 1993

[5] D. Cernomazu, Al. Simion, L. Mandici, "Electrostatic micromotors", pp. 88-93, Editura Universitatii Suceava, 1997

[6] C. Ungureanu, C. Bobric, D. Irimia, "Fuzzy Logic Control of a New Type of Electromagnetic Converter with Rolling Rotor," 12th International Conference on Applied and Theoretical Electricity, ICATE 2014 Craiova, October 23-25, 2014. [Online]. Available: http://dx.doi.org/10.1109/ICATE.2014.6972602

[7] H. Saavedra, J.-R. Riba, L. Romeral, "Multi-objective Optimal Design of a Five-Phase Fault-Tolerant Axial Flux PM Motor," Advances in Electrical and Computer Engineering, vol.15, no.1, pp.69-76, 2015, doi:10.4316/AECE.2015.01010

[8] H. Jussila, J. Nerg, J. Pyrhönen, A. Parviainen, "Concentrated Winding Axial Flux Permanent Magnet Motor for Industrial Use," International Conference on Electrical Machines, 2010. [Online]. Available: http://dx.doi.org/10.1109/ICELMACH.2010.5608168

[9] O. Dabija, A. Simion, L. Livadaru, N.D. Irimia, "Modeling and Simulation of an Axial Field Single-Pol Single-Phase Switched Reluctance Motor," 13th International Conference on Optimization of Electrical and Electronic Equipment, 2012. [Online]. Available: http://dx.doi.org/10.1109/OPTIM.2012.6231854

[10] V. Trifa, C. Marginean, "Preliminary Design of Reluctance Motors for Light Electric Vehicles Driving," Advances in Electrical and Computer Engineering, vol.9, no.1, pp.78-81, 2009, doi:10.4316/AECE.2009.01015

[11] T. Tudorache, L. Melcescu, "FEM Optimal Design of Energy Efficient Induction Machines," Advances in Electrical and Computer Engineering, vol.9, no.2, pp.58-64, 2009, doi:10.4316/AECE.2009.02009

[12] L. Livadaru, A. Simion, A. Munteanu, M. Cojan, O. Dabija, "Dual Cage High Power Induction Motor with Direct Start-up. Design and FEM Analysis," Advances in Electrical and Computer Engineering, vol.13, no.2, pp.55-58, 2013, doi:10.4316/AECE.2013.02009

[13] A. Malanciuc, A. Simion, L. Livadaru, A. Munteanu, C. Afanasov, "FEM-based Analysis of a Hybrid Synchronous Generator with Skewed Stator Slots," Advances in Electrical and Computer Engineering, vol.11, no.4, pp.9-14, 2011, doi:10.4316/AECE.2011.04002

[14] S. Sreeju Nair, N. Shamsuddeen, S.J. Dhinagar, "A Novel Electromagnetic Core Structure for Axial Radial Flux Permanent Magnet Electric Motor," IEEE 6th International Conference on Power Electronics, Machines and Drives, PEMD 2012. [Online]. Available: http://dx.doi.org/10.1049/cp.2012.0163

[15] Y. Niwa, Y. Akiyama, S. Manome, K. Miyazawa, "New Proposal of PM-Less Super-High-Speed Blower Motor," International Conference on Electrical Machines and Systems, ICEMS 2007, pp. 912-915

[16] B.J. Sung, E.W. Lee, J.G. Lee, "A Design Method of Solenoid Actuator Using Empirical Design Coefficients and Optimization Technique," Electric Machines & Drives Conference, IEMDC 2007. [Online]. Available: http://dx.doi.org/10.1109/IEMDC.2007.382679

[17] P. Wendling, P. Lombard, R. Ruiz et.al., "3D Motion in Magnetic Actuator Modeling," Proceedings of the 8th International Conference on Electrical Machines and Systems, ICEMS 2005, September 27-29. [Online]. Available: http://dx.doi.org/10.1109/ICEMS.2005.202605

[18] S. Banerjee, M.K. Sarkar, C. Chakraborty, "Analysis, Design, Fabrication and Testing of Three Actuators Based Electromagnetic Levitation System for Vehicle Application," IEEE Industrial Electronics Society, IECON 2013. [Online]. Available: http://dx.doi.org/10.1109/IECON.2013.6700338

[19] C. Ungureanu, A. Graur, "A Novel Design of a Rolling Rotor Actuator with Axial Air Gap," International Symposium on Fundamentals of Electrical Engineering, ISFEE 2014, Bucharest, [Online]. Available: http://dx.doi.org/10.1109/ISFEE.2014.7050557

[20] Flux® 9.1 2D Application, "User guide, Solving and results post-processing," 2005, vol. 4